Swelling In Light Water Reactor Internal Components: Insights from Computational Modeling

Roger E. Stoller[1,] Alexander V. Barashev[1,2], and Stanislav I. Golubov[1]

[1]Materials Science and Technology Division
Oak Ridge National Laboratory
Oak Ridge, TN 37831-6114, USA

[2]Center for Materials Processing
Department of Materials Science and Engineering
University of Tennessee, Knoxville, TN 37996-0750, USA

Prepared for:

August 2015
Oak Ridge National Laboratory

Abstract

A modern cluster dynamics model has been used to investigate the materials and irradiation parameters that control microstructural evolution under the relatively low-temperature exposure conditions that are representative of the operating environment for in-core light water reactor components. The focus is on components fabricated from austenitic stainless steel. The model accounts for the synergistic interaction between radiation-produced vacancies and the helium that is produced by nuclear transmutation reactions. Cavity nucleation rates are shown to be relatively high in this temperature regime (275 to 325°C), but are sensitive to assumptions about the fine scale microstructure produced under low-temperature irradiation. The cavity nucleation rates observed run counter to the expectation that void swelling would not occur under these conditions. This expectation was based on previous research on void swelling in austenitic steels in fast reactors. This misleading impression arose primarily from an absence of relevant data. The results of the computational modeling are generally consistent with recent data obtained by examining ex-service components. However, it has been shown that the sensitivity of the model's predictions of low-temperature swelling behavior to assumptions about the primary damage source term and specification of the mean-field sink strengths is somewhat greater that that observed at higher temperatures. Further assessment of the mathematical model is underway to meet the long-term objective of this research, which is to provide a predictive model of void swelling at relevant lifetime exposures to support extended reactor operations.

Contents

Nomenclature

3-D	–	three-dimensional or three-dimensionally;
dpa	–	displacements per atom;
EOS	–	equation of state;
LSODE	–	Livermore solver for ordinary differential equations;
NRT	–	standard for calculating displacements per atom (after authors M. Norgett, M. T. Robinson, and I. Torrens);
ODE	–	ordinary differential equations;

1.0   Introduction

This is the fifth report on our modeling-based investigation of radiation-induced microstructural evolution in the austenitic stainless steels used to fabricate commercial light water reactor internal components. The overall objective of this task is to develop a predictive model that can be used in lifetime assessments of these components. This is relevant to component lifetime in the nominal initial license period of about 40 years and is particularly important for considering the extended licensing periods of interest to the Light Water Reactor Sustainability (LWRS) program.

Since void swelling was discovered in the context of fast breeder reactor programs [1], most of the relevant experimental data has been obtained under conditions relevant to fast reactor operations and in experimental, sodium-cooled reactors. Although a broad database was developed, understanding of the phenomenon was limited by both the focus on the 350 to 650°C temperature window and the use of sodium-cooled test reactors. Due to the sodium melting temperature and thermodynamic considerations, the coolant inlet temperature in these reactors was typically in the range of 270 to 370°C which naturally determined the minimum temperature of any experimental data that was obtained. In addition, the neutron flux near the inlet elevation was lower than at the core mid-plane which meant that in any given experiment the lowest temperature data also accumulated less dose. The temperature and neutron fluence dependence of swelling database for fast reactor swelling conditions is illustrated in Fig. 1 [2,3]. The data and the predictions in this figure are for 20% cold-worked AISI 316 stainless steel (Fig. 1a is a variant of a figure in [3]). Results such as these were taken to imply that no significant swelling would develop below about 350°C. Although this inference was not well founded, it was often the basis for the assumption that swelling would not occur in the austenitic stainless steel structural core components of light water reactors (LWR).
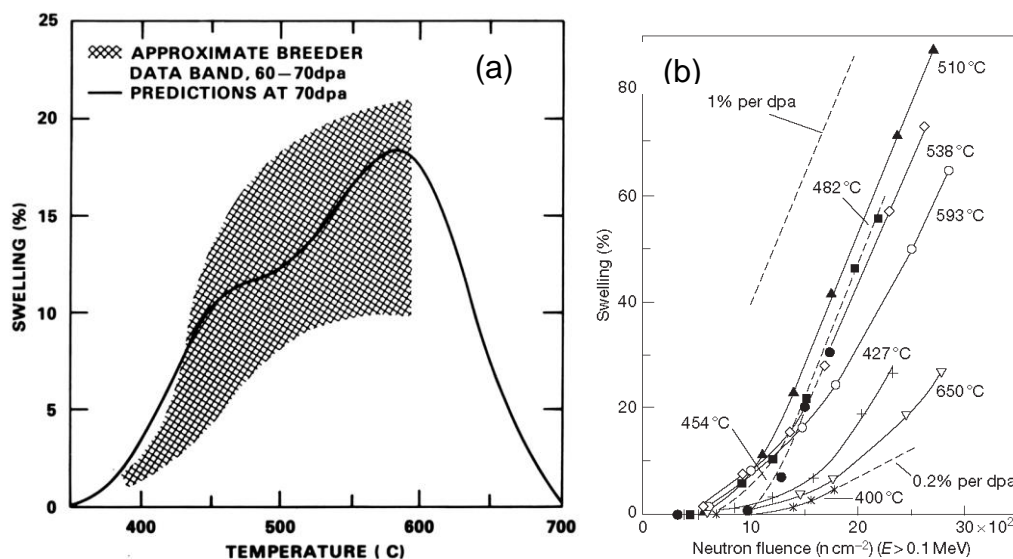

Figure 1:   Typical fast reactor swelling data for AISI 316 stainless steel showing temperature and neutron fluence dependence [2,3].

However, the issue of plant life extension has led to increasing discussion of the likelihood of swelling in LWR core components [4,5], and recent experimental observations make it clear that cavity formation and void swelling can occur in these materials. Post-irradiation examination of core components has provided many examples of cavity formation, although the level of swelling remains small for the exposure conditions examined so far. A representative example is shown in Fig. 2 of the voids observed during transmission electron microscopy of a baffle bolt taken from the Tihange pressurized water reactor (PWR) in Belgium [6]. Irradiation to 12 dpa at an estimated temperature of 345°C has produced about 0.2% swelling. The elevated temperature relative to the reactor coolant is a result of volumetric gamma heating, an issue that was not initially considered when component temperatures were estimated.
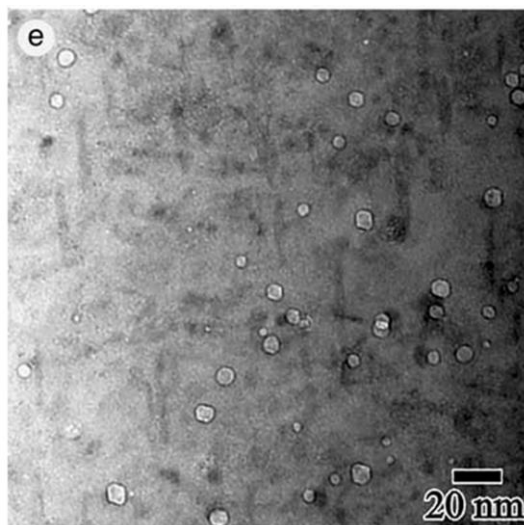

Figure 2:   Voids observed during TEM examination of baffle bolt from Tihange reactor in Belgium, figure reproduced from [6].

Since there is a substantial and growing body of experimental observations of cavity formation in LWR internal components after irradiation for much less than the initial licensing period of nominally 40 years, it is natural to be concerned about the potential for greater swelling which may occur during extended operation. A computational modeling and simulation effort was initiated to help provide interpretation of the data and guidance on the level of swelling that may be expected at high dose. The development and initial application of the model are described elsewhere [7,8]; this paper provides a summary of typical model predictions and some examples of the sensitivity of swelling to model parameters. It will be useful to define a few terms that are broadly used here and in the literature, i.e. cavity, bubble, and void. The term cavity is used generically to describe a small volume of empty space in the material; it may be either a bubble or a void. A bubble is a cavity which has sufficient gas content (typically helium in the materials of interest here) to stabilize it against vacancy emission which would otherwise be the thermodynamically dominant process due to the surface energy. A void is a cavity in which the gas pressure is too low to reduce vacancy emission. However, if voids manage to reach a critical size, the probability of vacancy emission is significantly reduced and these essentially empty cavities can also be stable in irradiated materials [3, 9]. Although it is common to characterize

radiation exposure in terms of neutron flux and fluence, the modeling results are more conveniently discussed in units of displacements per atom (dpa) and dpa rate. The transmutation-produced helium production can then be described as the ratio of helium production to displacement production in units of appm helium per dpa (He/dpa ratio).

2.0   Description of the Computational Model

The basis for the new model is a comprehensive microstructural model that was developed for similar materials in fast reactor fuel cladding [3]. That model employed the well-known reaction rate theory description of radiation damage formation and damage evolution, and explicitly accounted for the evolution of both the dislocation and cavity microstructures. The dislocation component includes the formation and growth of small interstitial loops which are known to be important at low to intermediate temperatures. The impact of helium produced by nuclear transmutation is observed in the nucleation of voids from an initial distribution of sub-critical bubbles.

Several areas were identified in which the base model required revision and further development to accurately describe the LWR environment; the principle areas were:

1. modify the description of primary radiation damage formation to account for recent advances in understanding based on atomistic simulations of damage production, i.e. point defect survival and clustering and interstitial cluster mobility [10],

2. provide an explicit bubble nucleation component based on a cluster dynamics description of He-vacancy clustering,

3. revise the reaction-diffusion components of the model to account for additional diffusion mechanisms and the relevant sink strengths for extended defects, i.e. mixed one- and three-dimensional diffusion of small interstitial clusters [11],

4. modify the primary radiation damage source terms in terms of displacements per atom (dpa) and helium production to account for the neutron energy spectrum, and

5. implement a recently developed approach for discretizing the interstitial loop size distribution to obtain greater accuracy.

Of the items in this list, numbers (1) to (3) are particularly significant. The initial model did not explicitly account for cavity nucleation. Based on microstructural data in the literature, a population of sub-critical bubbles was assumed to be present at the start of the simulations. This fixed density of bubbles could grow by helium and vacancy accumulation until they reached the critical size for bubble-to-void conversion [9]. Above this size, they began to grow more rapidly as voids. The weakness of this approach was the empirical (if experimentally guided) selection of the initial bubble population. The dose required for bubble nucleation is not accounted for in this scheme and it may become increasingly long for the low LWR temperatures. In addition, the model could not account for a realistic bubble size distribution. Therefore, a new cluster dynamics description of He-vacancy clustering has been developed to assess bubble nucleation. It can be used in a stand-alone fashion to compute the bubble size distribution at low doses, or it

can be incorporated into the comprehensive microstructural model.

Items (1) and (3) on the list are expected to be important for accurately describing the lower-temperature LWR irradiation conditions in which the density of small cascade-induced vacancy clusters, and hence their sink strength, is significantly higher than observed at the higher irradiation temperatures typical of FBR components. When the original model is used at temperatures below ~350°C, these transient vacancy clusters lead to an unphysical suppression of small interstitial dislocation. The high sink strength may also reduce bubble growth. Therefore, improving aspects of both primary radiation damage source terms and the kinetics of small interstitial clusters should lead to a more accurate description of the irradiated microstructure and its evolution at low temperatures.

2.1   Bubble nucleation model

The bubble nucleation model employs an extension of the accurate grouping scheme developed by Golubov and co-workers [12] which has been successfully used to simulate bubble evolution under post-irradiation annealing [13]. Briefly, the method solves the two-dimensional master equation describing He-vacancy clusters in a phase space defined by the variables x and m, which are the number of vacancies and helium atoms, respectively, in a cluster. We follow the commonly accepted assumption that a cluster of size x,m can change its size only by absorption and emission of monomers, e.g. single vacancies, self-interstitial atoms, or He atoms. In this case the master equation can be written as:

$$\frac{df(x,m,t)}{dt} = \left[J_x(x-1,m,t) - J_x(x,m,t) \right] + \left[J_m(x,m-1,t) - J_m(x,m,t) \right],\tag{1}$$

where

$$\begin{aligned} J_x(x,m,t) &= P_x(x,t)f(x,m,t) - Q_x(x+1,m,t)f(x+1,m,t)\,, \\ J_m(x,m,t) &= P_m(x,t)f(x,m,t) - Q_m(x,m+1,t)f(x,m+1,t)\,, \end{aligned}\tag{2}$$

and the coefficients $P_x(x,t), Q_x(x,m,t), P_m(x,t), Q_m(x,m,t)$ are the rates of capture and evaporation reactions between the monomers and clusters leading to a change in the size of clusters given by x and m.

In principle, it is possible to solve Eqn. (1) using an arbitrarily large set of discrete differential equations in the variables x and m. However, for bubble sizes typically observed experimentally, this would require a system of millions of equations because the number of equations must equal the product ($x \cdot m$). For example, a bubble radius of 2.0 nm requires the maximum value of x=3073 with potentially similar values of m. Practicable solutions of Eqn. (1) for relevant cases require developing a scheme for grouping the discrete size classes beyond a value of $x=m\sim10$. The grouping method used here has been shown to be highly accurate, conserving both the density of the extended defects (bubbles) in the size distribution, and the number of point defects contained in those the bubbles or voids (swelling). The method has been verified by comparison with exact analytical solutions for several cases [12, 13], and an example of the model's performance is shown in Fig. 3 [13].
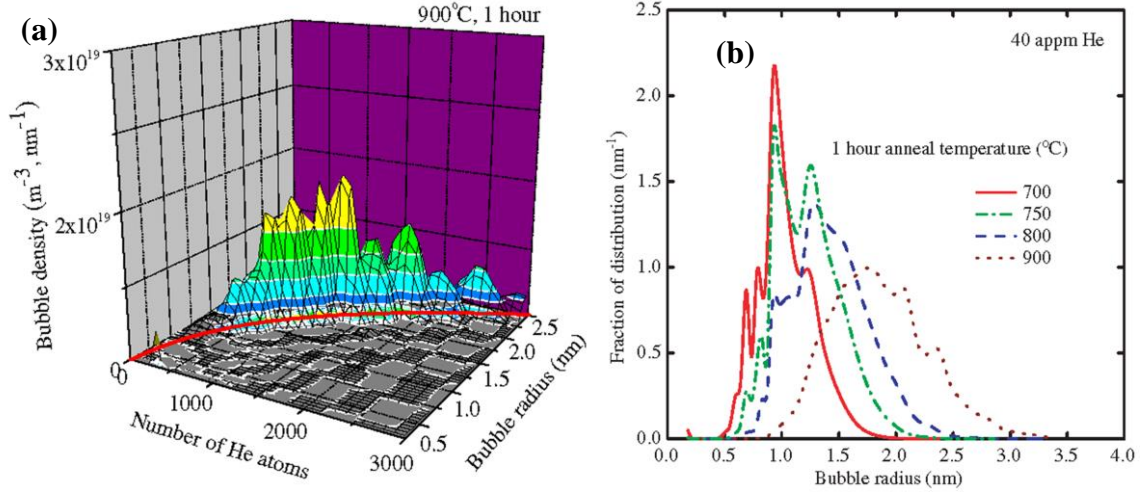
Figure 3: Example of results obtained for simulated post-irradiation annealing of He implanted austenitic stainless steel: (a) size distribution after annealing at 900°C and (b) temperature dependence of size distribution [13].

Based on the results of atomistic simulations [14], it is assumed that above certain maximum gas atom to vacancy ratio in the bubble, the bubble produces a Frenkel pair: one vacancy and one interstitial. This reaction can be defined as follows:

$$(x,m) + He \rightarrow (x+1, m+1) + i, \tag{3}$$

with the point defect generation properly accounted for in the rate equations for these species. The compressibility of helium in the bubbles is described using a hard-sphere equation of state [15, 16].

2.2 Other Components of Microstructural Evolution Model

2.2.1 Equations for Mobile Species

The concentrations, C, of mobile defects, vacancies (v), interstitials (i) and gas atoms (g) are described by the following typical equations:

$$\frac{dC_i}{dt} = G_i - \mu D_i C_i C_v - \left(z_i^d \rho_d + z_i^L k_L^2 + z_i^{GB} k_{GB}^2 + k_b^2\right) D_i C_i - 2w_1 D_i C_i^2 + \left(P^v f_L\right)_{x=2} + P_{FP}, \tag{4}$$

$$\frac{dC_v}{dt} = G_v - \mu D_i C_i C_v - \left(z_v^d \rho_d + z_v^L k_L^2 + z_v^{GB} k_{GB}^2 + k_b^2\right) D_v \left(C_v - C_v^e\right)$$
$$- w_1 D_g C_g C_v - 2w_1 D_v C_v^2 + \left(P^i f\right)_{x=2,m=0} + \left(Q^g f\right)_{x=1,m=1} + \left(Q^v f\right)_{x=2,m=0} \tag{5}$$

$$\frac{dC_g}{dt} = G_g - \left(z_g^d \rho_d + z_g^{GB} k_{GB}^2 + k_b^2\right) D_g C_g - w_1 D_g C_g C_v + \left(Q^g f\right)_{x=1,m=1} + \left(Q^i f\right)_{x=1,m=1}. \tag{6}$$

Here, μ is the recombination constant, ρ_d is the dislocation density, k_L^2, k_{GB}^2 and k_b^2, are the sink strength of interstitial loops, grain boundaries and gas bubbles, the Z_j^d are the capture efficiencies

of dislocations for vacancies (j=v), interstitials (j=i) and gas atoms (j=g), respectively. The Z_j^{GB} are corresponding capture efficiencies for grain boundaries, the G_j are the defect generation rates, and C_v^e is the thermal-equilibrium vacancy concentration. The P_{FP} term in Eq. (4) accounts for the formation of Frenkel pair from over-pressurized bubbles.

2.2.2   Other Extended Defects

The dislocation evolution model is described in detail in [3, 17]. In brief, the model described the homogeneous nucleation and growth of interstitial clusters that evolve into Frank faulted dislocation loops. At a critical size, which is determined by the mean spacing between dislocations, the loops unfault and become part of the dislocation network. At the same time, the initial network dislocation density can evolve by both thermal and radiation-induced climb processes which lead to annihilation of existing dislocations and formation of new dislocations. This model was shown to provide a good description of the evolution observed under irradiation in [3, 17]. The principle shortcoming of the model was mentioned in Item (5) above. A new description of loop evolution has been implemented which employs the improved grouping scheme of a one-dimensional master equation for the size distribution [12]. Both the network dislocations and faulted loops have a net bias for interstitials. The dislocation-interstitial bias is typically used as a fitting parameter in such work. As in the previous model [3], the bias exhibited by the two types of dislocations may be different, although they were set equal for the results reported here.

The previous microstructural model [3] included transient vacancy clusters in the form of very small microvoids. As first highlighted by Bullough and co-workers [18], these clusters act to suppress the vacancy supersaturation that would otherwise produce rapid nucleation of voids at low temperatures. In the updated model, these transient sinks are assumed to be vacancy loops rather than microvoids to distinguish their properties from the vacancy and He-vacancy clusters discussed above. The fraction of the initially-produced vacancies that are assigned to the vacancy loops is used as one fitting parameter.

As discussed in [3], the model assumes the existence of a small effective grain size which accounts for the coarse cell structure comprising microtwins, stacking faults and deformation bands observed in cold-worked materials. This effective grain size was treated as temperature dependent previously. Given the small range of temperature of interest here, the same value was used at each temperature.

3.0   Results of Simulations

Any kinetic model such as the one discussed here is necessarily incomplete in terms of accounting for all possible physical processes. Part of the art of model development is including enough detail to capture the primary mechanisms while ensuring that the model remains computationally tractable. In addition, the results will be sensitive to a range of material and irradiation parameters that can only specified within a certain range of uncertainty. This prevents the models from being truly predictive in an absolute sense. However, if the model parameters necessary to obtain agreement with a given data set can be determined, the model can be usefully

employed in a number of ways. For example, a well fit model will support limited extrapolations in exposure parameters temperature or dose (neutron fluence). Such a model can also be used to assess the significance of uncertainties regarding parameters and mechanisms. It may be the case that varying a material parameter within a reasonable range has little influence on the prediction of an integral parameter such as the swelling at a high dose. Similarly, the impact of individual mechanisms can be investigated to determine their significance.

In the following sections, the performance of the model with a given set of parameters will be demonstrated. Then variations of several model and irradiation parameters will be used to illustrate how they influence the predictions of the model. Because this model explicitly calculates the fluence dependence of several microstructural features: cavities, network dislocations, dislocation loops, and transient vacancy loops, the predictions of the model can be a complex function of some of these parameters. This is a result of the complex partitioning of mobile defect species between the extended defect sinks.

3.1 Results obtained with baseline parameter set

Table 1 lists the nominal or baseline set of material and irradiation parameters employed in the results shown below. The nominal material parameters such as the dislocation bias are taken from previous work investigating the swelling of 316 stainless steel at higher temperatures [3,19], and the irradiation parameters are representative of the service environment of LWR internal components. Simulations have been carried out over a range of temperatures to account for the gamma heating contribution to temperature in the thicker components. The temperature range was extended to 400°C to slightly overlap with earlier work that investigate swelling behavior under fast reactor conditions [3]. Although there is not sufficient data to support an extensive effort to refine the model parameters, reasonable agreement between the model and available swelling data was obtained with the values in Table 1. The sensitivity of a limited subset of model parameters are discussed here; these include the dislocation bias, the di-vacancy binding energy, the faction of cascade-produced vacancies in the transient vacancy loops, the helium generation rate, and the displacement rate.

Table. 1. **Nominal material and irradiation parameters (values in parentheses indicate those used in sensitivity studies)**		
Parameter	Value	Description
T	275; 300; 325; 400	Temperature (°C)
Ω	1.14×10^{-29}	Atomic volume (m^3)
g	1.65	Surface energy (J/m^2)
E_v^f	1.6	Vacancy formation energy (eV)
E_v^m	1.4	Vacancy migration energy (eV)
D_{v0}	8.0×10^{-7}	Vacancy diffusion coefficient (m^2/s)
D_{i0}	5.0×10^{-11}	Interstitial diffusion coefficient (m^2/s)
D_g	$8.0\times10^{-6}e^{(-0.7/kT)}$	He diffusion coefficient (m^2/s)
r_d	2×10^{15}	Initial network dislocation density (m^{-2})
Z_v, Z_i	1.0, 1.4 (1.25, 1.20)	Dislocation capture efficiencies
m/x_{max}	2	Maximum helium to vacancy ratio in bubbles
G_{NRT}	10^{-7} (10^{-4})	NRT generation rate (dpa/s)
ε_r	0.9	In-cascade recombination fraction
ε_v	0.1 (0.0)	Fraction of vacancies in vacancy loops
G_g	10^{-13}=1.0 ($5x10^{-14}$=0.5, $5x10^{-13,}$=5)	He generation rate (atom/s) and (appm/dpa)
E_{2V}	0.3 (0.25, 0.35)	Di-vacancy binding energy (eV)
R_g	10^{-6} m	Effective grain/sub-grain radius

The predicted dose dependence of the primary microstructural features is shown in Fig. 4 for temperatures between 275 and 400°C and doses up to 100 dpa. The figure includes void swelling (a), network dislocation density (b), interstitial loop density (c), and void density (d). Although the effect of temperature is clearly seen in the void density (d), the temperature sensitivity of swelling is not strong between 275 and 325°C. This effect increases significantly at higher temperatures as illustrated by the results at 400°C. The magnitude of the temperature effect on the dislocation components is similar. Less network recovery and loop densities are observed at the temperature increases. Based on the previous work with a similar model [3,19], proportionally greater network recovery is expected at temperatures higher than 400°C.
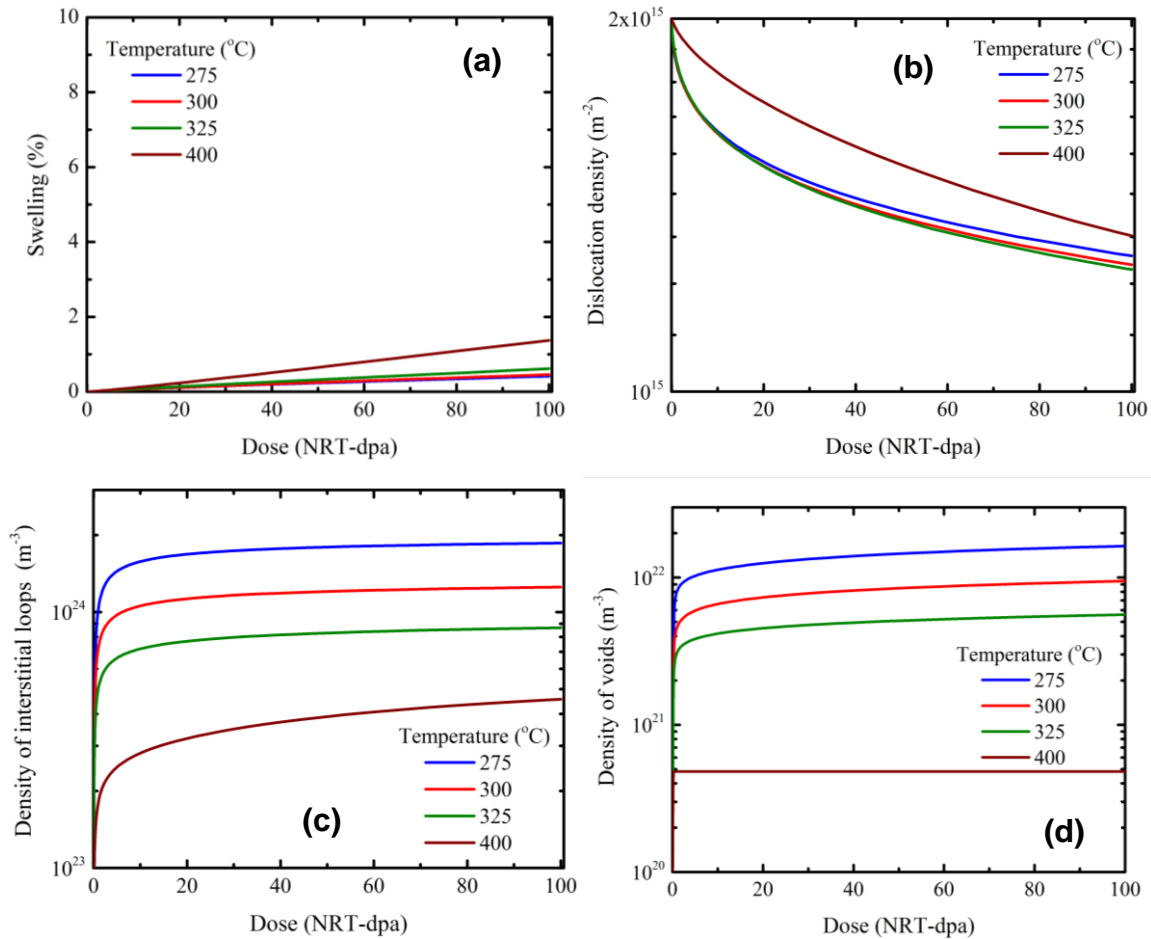

Figure 4: Dose dependence of void swelling (a), network dislocation density (b), interstitial loop density (c), and void density (d) using material and irradiation parameters from Table 1.

There is much less data available that can be used for model calibration and verification than the higher-temperature database that was developed by the large fast reactor programs in the 1970s and 1980s. The most important integral parameter is the total void swelling, and the model's predictions are consistent with the available data that tend to show a high density of small cavities with less than 1% swelling for doses up to ~80 dpa at temperatures near 300°C [20-23]. The minimum visible void and loop diameter is defined in the model as 1 nm. With this criterion, the loop density varies between 1.9×10^{24} and 8.7×10^{23} m^{-3} between 275 and 325°C. The

corresponding mean loop radii are 5.7 to 6.2 nm. For these same temperatures, the range in void density is 1.6×10^{22} and 5.6×10^{21} m^{-3}, with mean radii between 3.8 and 6.2 nm. The experimental results reported in the literature are often a bit vague for the small microstructural features, listing a mean "size" without specifying whether this is a radius or diameter. With the current model parameterization, it appears that the loop and void densities are within an order of magnitude of most measurements. The mean loop radii are a factor of 2 to 5 smaller and the void radii a factor of 2 to 5 larger than at least some of the observations. Improved agreement with specific experiments could be obtained by varying model parameters, but the overall agreement is satisfactory.

3.2 Influence of helium generation

The austenitic stainless steels used to fabricate LWR internal components contain a substantial amount of nickel, and the neutron energy spectrum in the core includes a significant fraction of thermal neutrons. These two facts mean that the helium generation rate is not a constant, but starts at a low level and increases as the thermal neutrons transmute ^{58}Ni into ^{59}Ni, and thermal neutrons subsequently produce helium via an (n,α) reaction on ^{59}Ni [24], i.e.

$$^{58}\text{Ni(n,}\gamma)^{59}\text{Ni(n,}\alpha)^{56}\text{Fe.} \tag{7}$$

This nonlinear, dose or fluence-dependent He generation rate has the potential to alter the critical process of bubble nucleation at low doses. For 316 stainless steel with a nominal nickel content of 12 weight-%, exposure to a typical displacement rate of 5×10^{-8} dpa/s in a LWR neutron energy spectrum leads to an initial helium generation rate of about 0.5 appm/dpa which increases to more than 10 appm/dpa by about 60 dpa (~5×10^{22} n/cm^2, E>1 MeV). This non-linear generation has been assessed as a result of a collaboration with Dr. L. R. Greenwood of Pacific Northwest Laboratory that provided the dose dependence of the He/dpa ratio as described in [7]. Because the bubbles tend to nucleate early when the helium generation rate is low, the cavity density was less sensitive than expected. The density and swelling with the dose dependent He/dpa ratio was nearly the same as that obtained with a constant value of 1.0 appm He/dpa, the value specified in Table 1. Figure 5 shows the dependence of swelling and void
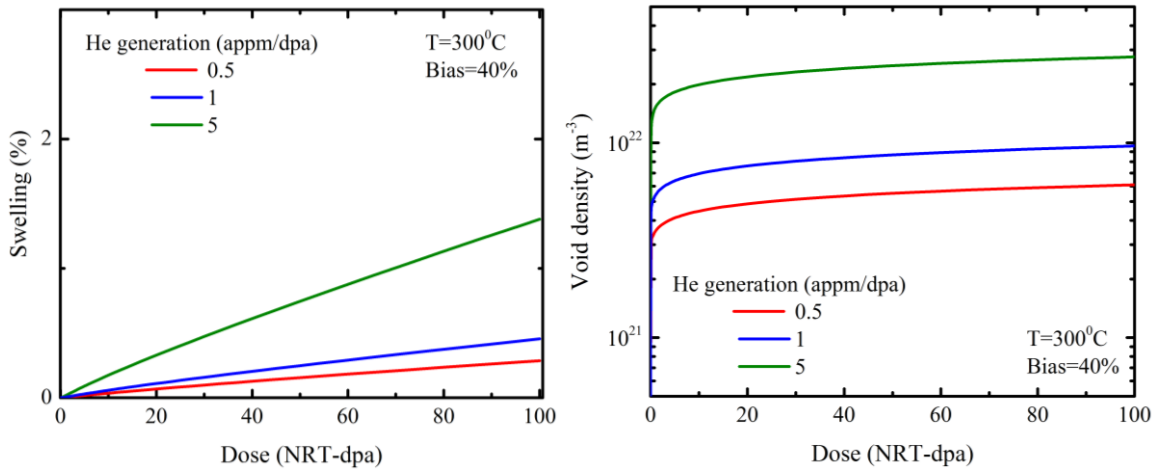

Figure 5: Dose dependence of void swelling (a) and void density (b) using material and irradiation parameters from Table 1 but showing sensitivity to the He/dpa ratio, c.f. Fig. 1a and 1d.

density at 300°C using different constant He/dpa ratios to illustrate the potential sensitivity of these parameters. The impact of helium increases for values greater than 1 to 2 appm/dpa. Although the He/dpa ratio will vary depending on the local energy spectrum and flux, these values are representative. Hydrogen is also generated by (n,p) reactions [24,25] and may contribute to bubble stabilization. Only a limited amount of research has been devoted to how hydrogen could act synergistically with He to influence microstructural and mechanical property changes under irradiation. The results in [26] indicate that hydrogen may have some influence at high concentrations, but the effect of hydrogen is not included in the model.

3.3 Influence of sink density and sink strengths

Figures 6 and 7 illustrate the sensitivity of the model to the dislocation bias and the transient vacancy clusters, respectively. As discussed in [19], the results of elasticity calculations have suggested values of the bias ranging from 1% to almost 100%. Thus, the values of 25 and 40% are mid-range relative to the calculated bias. Reducing the bias from 40% to 25% reduces the predicted swelling almost proportionally; note the scale of ordinate is reduced in Fig. 5a compared to Fig. 4a. There is little change in the loop or void density. The absolute amount of dislocation network recovery is very similar to the 40% bias case at 275 to 325°C. However, at 400°C there is a more significant increase in network dislocation recovery.
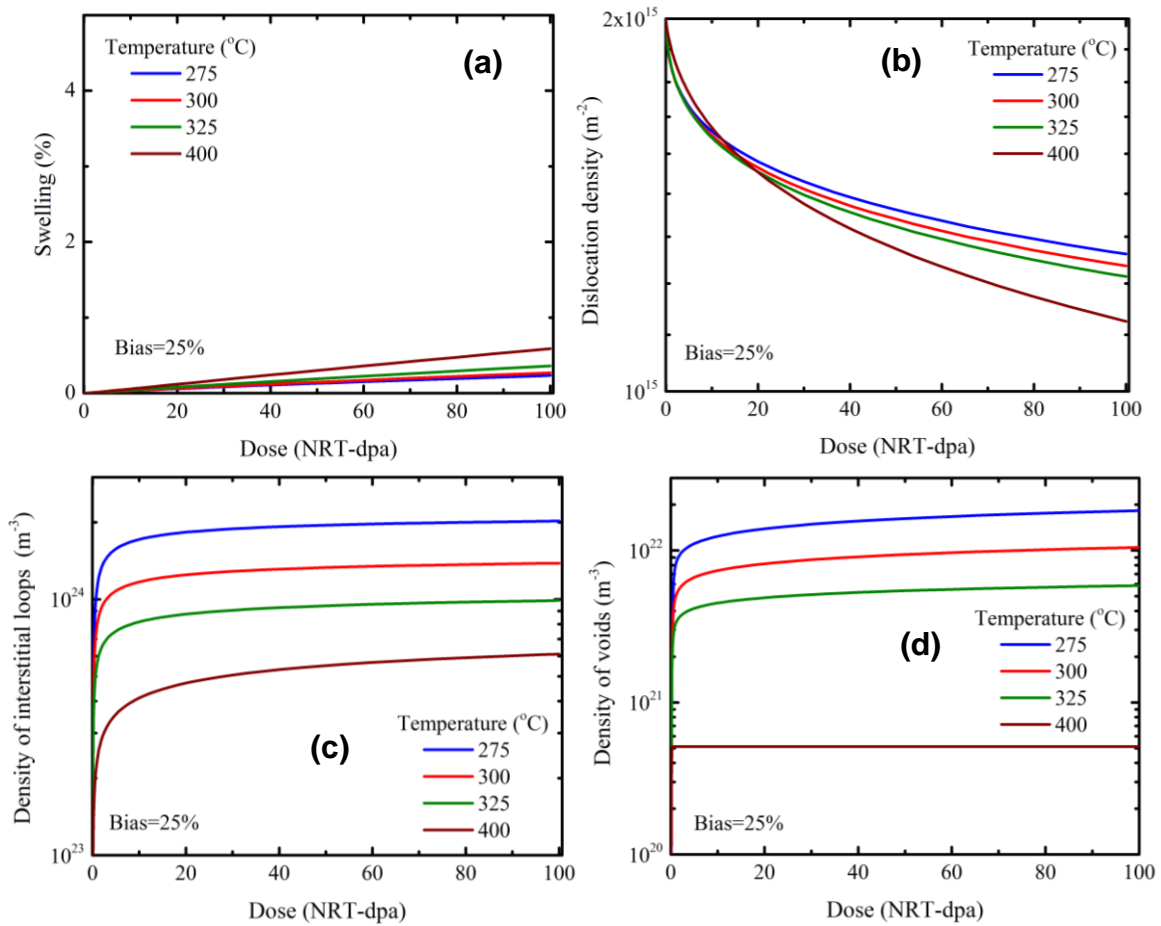

Figure 6: Dose dependence of void swelling (a), network dislocation density (b), interstitial loop density (c), and void density (d) using material and irradiation parameters from Table 1, except dislocation bias reduced to 0.25.

The significance of the transient vacancy loops in suppressing the vacancy supersaturation was already mentioned. This is illustrated in Fig. 7 for the temperatures of 275 and 325°C. The effect is most dramatic at 275°C where the cavity density increases by more than a factor of two and the swelling by a bit more than an order of magnitude. The reduction in swelling with decreasing temperature observed in Fig. 1a is reversed with much higher swelling predicted at 275 than 325°C. The necessity of including such a transient defect does not mean such a sink is physically present in the material. Rather, they may act a surrogate for a missing mechanism in such models or may account for a failure of the mean field models to account for some unspecified spatially dependent defect reactions.
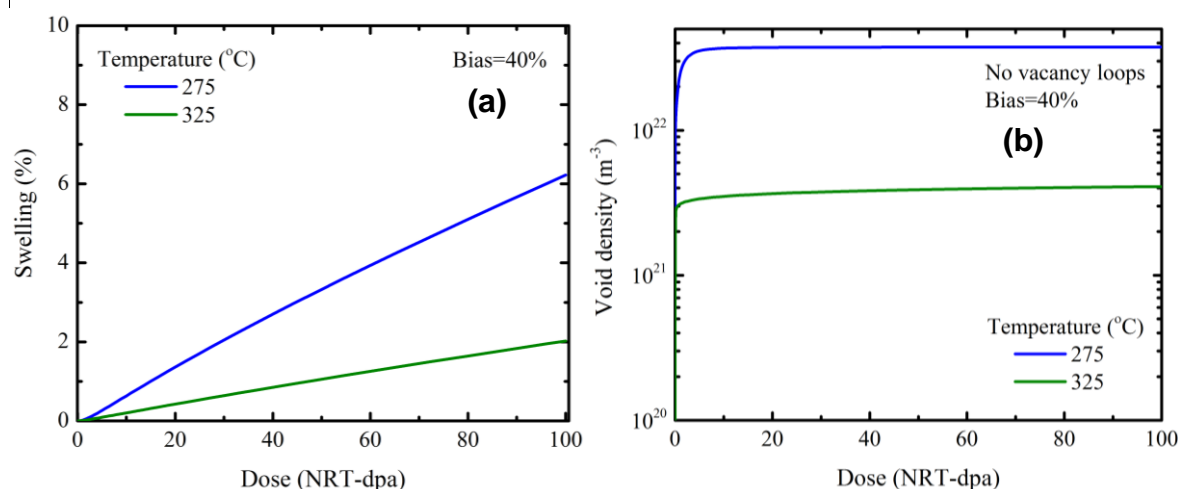

Figure 7: Dose dependence of void swelling (a) and void density (b) using material and irradiation parameters from Table 1 but showing sensitivity to the transient vacancy loops, c.f. Fig. 4a and 4d.

Void nucleation is typically very sensitive to the di-vacancy binding energy is because this parameter establishes the basic stability of vacancy clusters. In a simple cluster dynamics model, one expects that lower binding energies would reduce the void density, and would like reduce swelling. However, because of the high sink strengths and complicated interplay between point defects and extended defects, the behavior with the current model is more complex. Figure 8 illustrates the sensitivity of the predicted swelling (a) and (c) and void density (b) and (d) to modest variation in the di-vacancy binding energy. Figure 8 (a) and (b) show results which include the influence of transient vacancy clusters while parts (c) and (d) do not.

In contrast to the simple dependence just mentioned, the void swelling behavior shown in Fig. 8(a) is not a monotonic function of the di-vacancy binding energy. At 275°C it is highest with the highest binding energy but at 300°C and above it is lowest with the highest binding energy. The void density in Fig. 8(b) is only sensitive to this parameter at the lowest and highest temperatures, and only at 275°C is the void density higher for the highest binding energy. This behavior is largely due to the fact that the di-vacancy binding energy influences the evolution of both the cavities and the transient vacancy loops, and their relative sink strengths can change as a function of temperature and the binding energy. The behavior is more simple when the transient vacancy loops are not included as shown in Fig. 8(c) and (d). At the lower temperatures the swelling and

void density both increase as the binding energy increases. However, as noted when Fig. 7 was discussed, the low-temperature swelling is much higher than expected in this case.
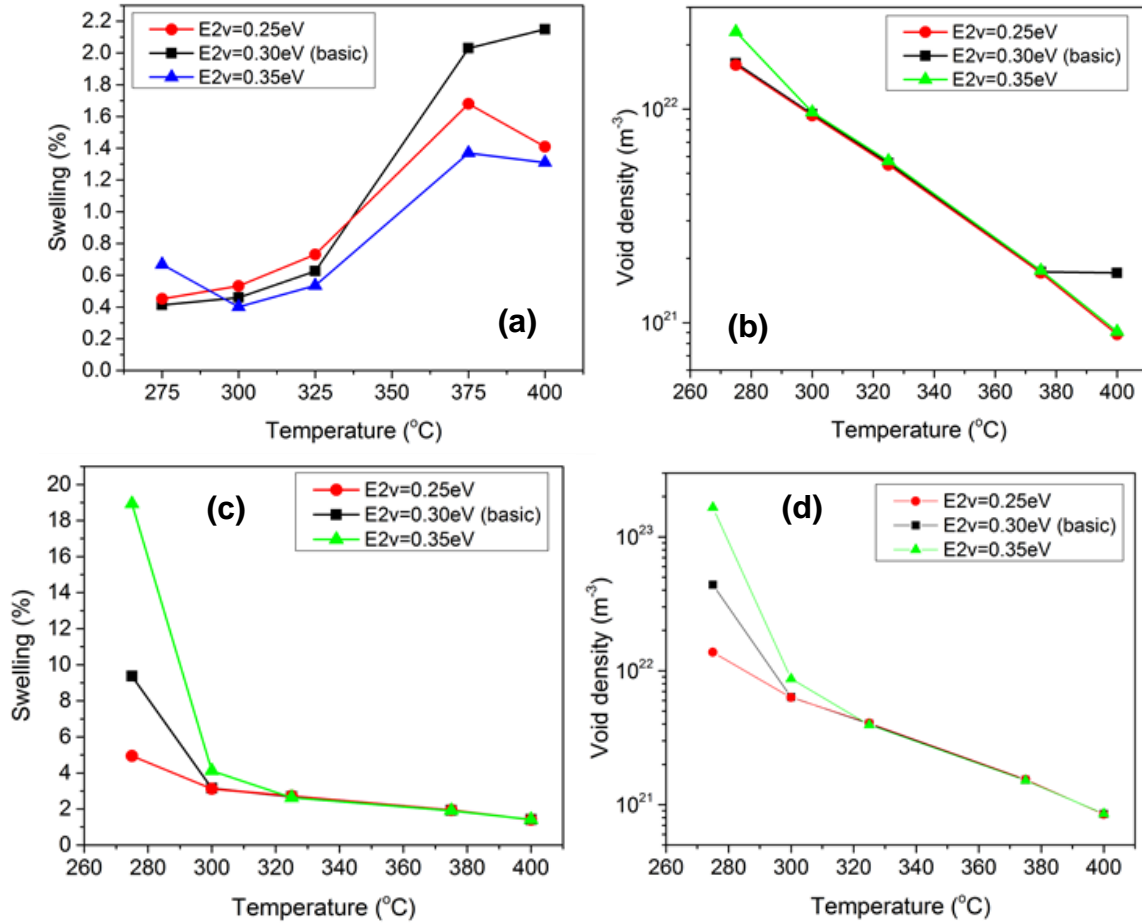

Figure 8: Temperature dependence of swelling (a) and (c) and void density (b) and (d) at 100 dpa. Transient vacancy clusters are included in (a) and (b) but not in (c) and (d).

3.4 Influence of displacement rate

The characteristic displacement rate for LWR internals is $\sim 10^{-7}$ dpa/s as listed in Table 1. However, ion irradiations at much higher displacement rates are commonly used in order to reach high doses in relatively short times. Previous research has established a link between displacement rate and irradiation temperature that can be used to obtain a comparable irradiation response under different irradiation conditions [27-29]. However, these correlations were generally established for conditions related to the peak swelling temperature, $\sim 550°C$ in the austenitic stainless steels, where the density of extended defects is much lower. Under these conditions, an increase in damage rate tends to reduce swelling due to the increase in sink density and a higher irradiation temperature must be used to reduce the sink strength and obtain swelling behavior similar to the lower damage rate result. This leads to the well-known "temperature shift" correlations [27-29].

The model indicates that the behavior may be somewhat different under low-temperature irradiation conditions that lead to a high sink density at low damage rates. The results obtained at 10^{-7} and 10^{-4} dpa/s are shown in Fig. 9; both swelling (a) and void density (b) are shown as a

function of temperature at 100 dpa. Simulations were carried out in which the transient vacancy clusters were included and without these vacancy clusters. In both cases the swelling is increased significantly at the higher damage rate, with the increase being greater at the lower temperatures.
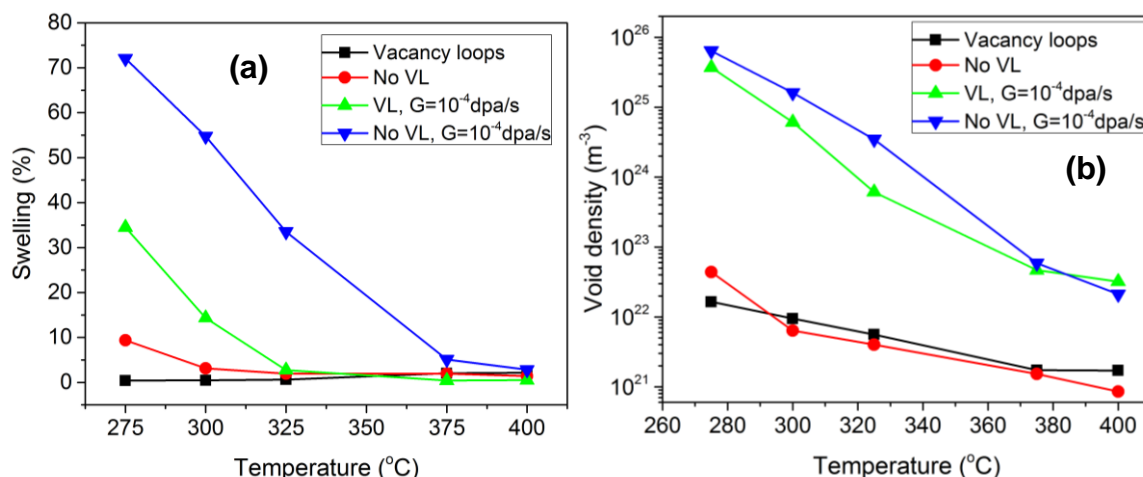

Figure 9: Influence of displacement rate on void swelling (a) and void density (b) at 100 dpa.

This is a result of substantial increases in the void density as shown in (b). Only at the highest temperatures shown is the swelling reduced at the high displacement rate as the temperature-shift model would predict.

4.0   Conclusions

A recently revised and improved mean-field reaction rate theory model has been applied to investigate the potential for swelling of austenitic stainless steels at high doses under exposure conditions relevant to LWR internal components. With a given parameterization, the predictions of the model are broadly consistent with the available microstructural data such as measurements of swelling, and the density of faulted interstitial loops and cavities. Although the model predictions are sensitive to a range of material and irradiation parameters, they suggest that more significant swelling is likely to occur as the irradiation exposure increases during extended operation. Greater swelling is predicted for components that exceed the nominal 290°C LWR operating temperature. Since it is possible that the so-called swelling incubation time is extremely long under such low temperature irradiation, it is conceivable that exposure to much higher doses will lead to the high swelling rates observed in the 400 to 650°C temperature range [2]. Some analysis suggests that this is not likely [30], but further work is required to assess this possibility.

The high vacancy supersaturations obtained under low-temperature irradiation suggest that void nucleation should be very easy. This is somewhat in contradiction to the experimental observations. Further investigations are underway to develop a better understanding of nucleation mechanisms in this regime.

5.0   Future Work

The requirement for the postulated transient vacancy cluster to reduce low-temperature swelling [3, 18] is somewhat of an *ad hoc* fix and requires further research. First, the applicability of the effective medium, mean field sink strengths used in such models [31] needs to be assessed for the very high sink densities that are observed at low temperatures. These high sink densities are also characteristic of the high damage rate ion irradiations that are used to obtain high-dose data. We are addressing two possibilities. First, the impact of including the higher-order, multiple sink corrections discussed in Ref. [31] will be assessed. This will effectively increase the absorbing power (strength) of each sink relative to its physical dimensions. In addition, the sink correction terms will increase the sink strength of each sink for interstitials more than for vacancies. In this case, the "neutral" sinks such as cavities and grain boundaries will no longer be neutral. We will also investigate the possible impact of the dissolution of fine defect clusters by displacement cascades since this may limit the maximum achievable density of these clusters.

REFERENCES

[1]   Cawthorne, C., and Fulton, E. J. "Voids in irradiated stainless steel," Nature 216 (1967) 575-576.

[2]   Garner, F. A. "Radiation Damage in Austenitic Steels," in Comprehensive Nuclear Materials, Vol. 4, R. J. M. Konings, T. R. Allen, R. E. Stoller, and S. Yamanaka, Eds., Elsevier Ltd., Amsterdam, 2012, pp. 33-95.

[3]   Stoller, R. E., and Odette, G. R. "A composite model of microstructural evolution in austenitic stainless steel under fast neutron irradiation," Radiation Induced Changes in Microstructure: 13th International Symposium, ASTM STP 955, F.A. Garner, N.H. Packan, and A.S. Kumar, Eds., American Society for Testing and Materials, Philadelphia, 1987, pp. 371-392.

[4]   Garner, F. A., Greenwood, L. R., and Harrod, D. L. "Potential High Fluence Response of Pressure Vessel Internals Constructed from Austenitic Stainless Steels', in Sixth Intern. Symp. on Environmental Degradation of Materials in Nuclear Power Systems – Water Reactors, TMS, Warrandale, 1993, pp. 783–790.

[5]   Garner, F. A. "Void Swelling and Irradiation Creep in Light Water Reactor Environments," in Understanding and Mitigating Ageing in Nuclear Power Plants, Woodhead Publishing Limited, Oxford, 2010, pp. 308-356.

[6]   Edwards, D. J., Simonen, E. P., Garner, F. A., Greenwood, L. R., Oliver, B. A., and Bruemmer, S. M. "Influence of irradiation temperature and dose gradients on the microstructural evolution in neutron-irradiated 316SS," J. Nucl. Mater. 317 (2003) 32–45

[7]   Stoller, R. E., Barashev, A. V., and Golubov, S. I. "Low-temperature Swelling in LWR Internal Components: Current Data and Modeling Assessment," Oak Ridge National Laboratory, ORNL/LTR-2012/390, Sept. 2012.

[8]   R. E. Stoller, A. V. Barashev, and S. I. Golubov," The Influence of Helium on Low-temperature Swelling in LWR Internal Components," Oak Ridge National Laboratory, ORNL/LTR-2013/200, May, 2013.

[9]   Stoller, R. E. and Odette, G. R. "A Comparison of the Relative Importance of Helium and Vacancy Accumulation in Void Nucleation," Radiation-Induced Changes in Microstructure, 13th International Symposium, ASTM STP 955, F. A. Garner, N. H. Packan and A. S. Kumar, Editors, American Society of Testing and Materials, Philadelphia, 1987, pp. 358-370.

[10]   Stoller, R. E. "Primary Radiation Damage Formation," in Comprehensive Nuclear Materials, R. J. M. Konings, T. R. Allen, R. E. Stoller, and S. Yamanaka, Editors, Elsevier Ltd., Amsterdam, 2012, pp. 293-332.

[11]   Golubov, S. I., Barashev, A. V., and Stoller, R. E. "Radiation Damage Theory," in Comprehensive Nuclear Materials, R. J. M. Konings, T. R. Allen, R. E. Stoller, and S. Yamanaka, Editors, Elsevier Ltd., Amsterdam, 2012, pp. 357-391.

[12] Golubov, S. I, Ovcharenko, A. M, Barashev, A. V., and Singh, B. N. "Grouping method for the approximate solution of a kinetic equation describing the evolution of point-defect clusters," Phil. Mag. A 81 (2001) 643-658.

[13] Golubov, S. I, Stoller, R. E, Zinkle, S. J., and Ovcharenko, A. M. "Kinetics of coarsening of helium bubbles during implantation and post-implantation annealing," J. Nucl. Mater. 361 (2007) 149-159.

[14] Stewart, D. M., Osetsky, Yu. N., Stoller, R. E., Golubov, S. I., Seletskaia, T., Kamenski, P. J. "Atomistic Studies of Helium Defect Properties in BCC Iron: Comparison of He-Fe Potentials," Phil. Mag. 90 (2010) 935-944.

[15] Brearley, I. R., and MacInnes, D. A. "An improved equation of state for inert-gases at high-pressures," J. Nucl. Mater. 95 (1980) 239-252.

[16] Stoller, R. E. and Odette, G. R "Analytical Solutions for Helium Bubble and Critical Radius Parameters Using a Hard Sphere Equation of State," J. Nucl. Mater.131 (1985) 118-125.

[17] Stoller, R. E. "Modeling Dislocation Evolution in Irradiated Alloys," Met. Trans. 21A (1990) 1829-1837.

[18] Bullough, R,. Eyre, B. L., and Krishan, K. "Cascade damage effects on swelling of irradiated materials," Proceedings of the Royal Society of London A 346 (1975) 81-102.

[19] Stoller, R. E. "Microstructural evolution in fast-neutron-irradiated austenitic stainless steels," ORNL-6430, Oak Ridge National Laboratory, December, 1987.

[20] Chung, H. M. "Assessment of void swelling in austenitic stainless steel core internals," NUREG/CR-6897, ANL-04/28, Argonne National Laboratory, December, 2004.

[21] Porollo, S. I., Dvoriashin, A. M., Konobeev, Yu. V., Ivanov, A. A., Shulepin, S. V. and Garner, F. A. "Microstructure and mechanical properties of austenitic stainless steel 12X18H9T after neutron irradiation in the pressure vessel of BR-10 fast reactor at very low dose rates, "J. Nucl. Mater. 359 (2006) 41-49.

[22] Edwards, D.J., Simonen, E. P., and Bruemmer, S. M., "Evolution of fine-scale defects in stainless steels neutron-irradiated at 275°C," J. Nucl. Mater. 317 (2003) 13-31.

[23] Edwards, D.J., Simonen, E. P., Garner, F. A., Greenwood, L. R., Oliver, B. M. and Bruemmer, S. M. "Influence of irradiation temperature and dose gradients of the microstructural evolution of neutron-irradiated 316SS," J. Nucl. Mater. 317 (2003) 32-45.

[24] Greenwood, L. R. "A new calculation of thermal neutron damage and helium production in nickel," J. Nucl. Mater. 115 (1983) 137-142.

[25] Garner, F. A., Oliver, B. M., Greenwood, L. R., Edwards, D. J., Bruemmer, S. M. and Grossbeck, M. L. "Generation and retention of helium and hydrogen in austenitic steels irradiated in a variety of LWR and test reactor spectral environments," Fusion Reactor Materials: Semi-Annual Progress Report Ending June 30, 2001, DOE Office of Fusion Energy Sciences, Washington DC, pp. 127-147.

[26] Hunn, J. D., Lee, E. H., Byun, T. S., and Mansur, L. K. "Helium and hydrogen induced hardening in 316 LN stainless steel," J. Nucl. Mater. 282 (2000) 131-136.

[27] N. H. Packan, K. Farrell, and J. O. Stiegler, "Correlation of neutron and heavy-ion damage: I. The influence of dose rate and injected helium on swelling in pure nickel," J. Nucl. Mater. 78 (1978) 143-155.

[28] L. K. Mansur, "Correlation of neutron and heavy-ion damage: II. The predicted temperature shift of swelling with changes in radiation dose rate," J. Nucl. Mater. 78 (1978) 156-160.

[29] N. M. Ghoniem, "The effect of damage rate on void growth in metals," J. Nucl. Mater. 82 (1979) 392-402.

[30] Garner, F. A. "Assessment of the swelling equation used to predict swelling of AISI 304 stainless steel in LWR and LMR environments," Proceedings of 16th International Conference on Environmental Degradation of Materials in Nuclear Power Systems - Water Reactors, 2013 (in CD format, no page numbers).

[31] A. D. Brailsford, A. D. and Bullough, R. "The theory of sink strengths," Philosophical Transactions of the Royal Society of London A 302, (1981) 87-137.